ADVANCED FUNCTIONAL MATERIALS
www.afm-journal.de

Reprogrammable 4D Printed Liquid Crystal Elastomer Photoactuators by Means of Light-Reversible Perylene Diimide Radicals

*Lorena Montesino, Jesús I. Martínez, and Carlos Sánchez-Somolinos**

Reconfigurable soft actuators can be programmed to morph into different 3D shapes under the same stimulus exhibiting great potential for adaptive robotic functionalities. Liquid crystalline crosslinked materials programmed and controlled by light have demonstrated great potential in this area, however, their implementation is mainly based on azobenzene chromophores, using ultraviolet light that can potentially damage the device and its surroundings, especially if living cells are present. Here, an ink is presented, containing a green-absorbing perylene diimide chromophore, to prepare light active liquid crystalline elastomer (LCE) actuators via direct ink writing. Green light irradiation of the LCE elements leads to photothermal actuation, but also to new absorption bands in the far-red and near-infrared, ascribed to the formation of radical species. Far-red irradiation results in mechanical actuation and, advantageously, a recovery of the original absorption spectrum. This reversible transformation enables spatial reconfigurability of the actuator's response to far-red light. The reconfigurable system gives access to complex deformation modes by simply exciting the element with homogeneous far-red light, without the need for any structural modification of the actuator. This material strategy, using green and far-red light, less harmful than ultraviolet, shows significant promise for future development of reconfigurable actuators for biomedical applications.

1. Introduction

Reproducing the wide variety of delicate and highly complex movements observed in nature has been one of the most sought-after goals in the field of soft robotics in recent years.[1–4] Liquid crystal elastomers (LCEs) are being widely explored as one of the main families of materials to reach this objective.[5–11] When exposed to appropriate external stimuli, such as for example heat or light, these materials exhibit large anisotropic mechanical responses because of the change in the molecular order of the liquid crystal constituent molecules. In this way, an increase in temperature induces liquid crystal disorder in the system leading to contraction along the molecules' preferential orientation direction, the director **n**, while the system expands in the orthogonal directions.[12–14] The control over the configuration of the director, which can be achieved with a high degree of complexity, has been thoroughly explored as a tool to prescribe the modes of actuation in LCEs.[15–20] Different approaches have been developed for this purpose, including those processing methodologies based on surface-enforced techniques, field-assisted procedures, mechanical tools, and rheological strategies.[21] Among rheological methods, 4D printing has recently arisen as a promising technique to digitally define a given director pattern in the LCE actuator.[22–25] Nevertheless, all the previously mentioned processing techniques typically result in single-mode actuators, when using a single material in the preparation and a homogeneous stimulus in the excitation. This aspect supposes a strong constraint to attain the multitude of degrees of freedom of the natural movements that are to be emulated. Living organisms display adaptive movements that can vary depending on environmental inputs. Therefore, it is highly desirable to create multimodal soft actuators, that can be programmed to change their shape morphing mode even in front of a single and homogeneous stimulus. This approach, which brings us one step closer to simulating the multitude of movements that we observe in nature, might directly be associated with a reversible programming step of the actuator. In this context, the development

L. Montesino, J. I. Martínez, C. Sánchez-Somolinos
Instituto de Nanociencia y Materiales de Aragón (INMA)
Departamento de Física de la Materia Condensada
CSIC-Universidad de Zaragoza
Zaragoza 50009, Spain
E-mail: carlos.s@csic.es

C. Sánchez-Somolinos
Centro de Investigación Biomédica en Red de Bioingeniería
Biomateriales y Nanomedicina
Instituto de Salud Carlos III
Zaragoza 50018, Spain

The ORCID identification number(s) for the author(s) of this article can be found under https://doi.org/10.1002/adfm.202309019

DOI: 10.1002/adfm.202309019

of ways for easy and reconfigurable programming of the material becomes meaningful.

The most frequent reconfiguration strategies in stimuli-responsive systems are based on the modification of covalent bonds or the introduction of molecular changes.[26–33] The local application of such changes, typically mediated by chemical reactions, presents significant challenges, being therefore not straightforward to achieve a simple and spatially well-defined reconfiguration of the modes of actuation. To tackle this setback, light-mediated programming processes burst in as a powerful strategy, being able to induce the previously mentioned modification of bonds, as well as to trigger other conformational modifications of photoswitches such as the hemithioindigos or azobenzenes, with high spatial and temporal control.[34–36] Focusing on these last ones, the light-induced conformational change between the *trans* and the *cis* state of azobenzene units incorporated into the polymeric network can disrupt the original liquid crystal order, leading to a structural modification of the material. The photochemical generation of long-lived *cis* isomers in the material has been used as a programming tool, as this change introduces modifications in the mechanical properties of the irradiated material. Subsequent photothermal stimulus induces actuation of the system and therefore a shape morphing that is conditioned by the programming step. After the actuation step, it is possible to reconfigure the system again by performing a new programming step toward a new actuation mode.[37] The use of these photochemical switches presents the advantage of having a high spatio-temporal control of the reconfiguration, as the conversion between the two states of the molecules can be achieved through a photochemical path with the light of two different wavelengths, which are usually in the range of the ultraviolet (UV) and visible (Vis) regions of the electromagnetic spectrum. However, the use of these well-extended two-state molecules in one of the main fields in which the application of soft robotics is crucial, biomedicine, can be precisely limited by the light bands which they can absorb.[35] When living cells are involved in the operation of biomedical devices, UV light, which would be needed to control the deformation of actuators, could damage the genetic material of the cells, inducing mutations that could alter cell behavior and even trigger apoptosis processes.[38] Thus, an effort needs to be done on shifting the absorption peaks of molecular switches to less harmful wavelengths in the visible or infrared (IR) part of the spectrum.[39,40] Advantageously, IR light represents not only an innocuous source of light for cells, but it also takes benefit of the near-infrared (NIR) windows of the biological tissues.[41] This condition makes the Vis-IR region quite appealing for biological applications. This aspect has led research to focus on the development of molecules capable of operating in this region of the spectrum, which can be incorporated into solid matrices, as in the case of the indigo chromophore and its derivatives.[42]

Herein, we report the development of a printable ink, based on a perylene diimide chromophore, to prepare light-driven and light-reconfigurable LCEs. The photoactive film presents a strong absorption in the green region of the visible spectrum, therefore leading to shape changes triggered by photothermal effects under green light. Concurrently, we have observed that this exposure to green light results in a change in the absorption spectrum of the material, with the appearance of strong absorption bands in the far-red and NIR. This opens the possibility to induce deformation via photothermal effect with light in these regions of the spectrum. Advantageously, immediate irradiation of the LCE with light in these far-red or NIR bands reverts the system to its original absorption spectrum. This light-induced conversion of the material between two states of different absorption, together with the ability of 4D printing to digitally define the director, can give access to reconfigurable complex actuators leading to different accessible shape morphing states under homogeneous irradiation with a light source in the far-red or NIR regions of the spectrum.

2. Results and Discussion

2.1. Ink Preparation

To obtain the LCE actuators under study in this work, inks composed of a reactive liquid crystalline macromer with acrylate groups at the extremes of the chain polymer and a photoinitiator molecule were first prepared. Details on the chemical composition are shown in **Figure 1**A. The LCE oligomer was synthesized by the Michael addition of *n*-butylamine to the mesogenic diacrylate RM82 in a 1:1,02 molar ratio as previously reported.[23] The slightly lower stoichiometric amount of *n*-butylamine compared to diacrylate allows both reaching long macromer chains that facilitate to get a proper alignment of the polymer chains during the printing process, and retaining acrylate functionalities at the end of the polymeric chains that enable the polymerization in a second step mediated by a light-initiated free-radical photopolymerization. The choice of this ratio between the two components seeks the formation of less cross-linked final elastomeric systems to obtain significant actuation at temperatures that can be typically achieved at reasonable light intensities when dyes are incorporated into the system. As a trigger molecule for the photopolymerization process, IRG369 was added in a proportion of 1 wt.%. Such selection was done based on previous results of the group, leading this percentage to effective elastomer formation.[23] As photoactive unit to transduce light into heat in our LCE, a perylene dye, N,N′-Bis(2,6-diisopropylphenyl)−3,4,9,10-perylenetetracarboxylic Diimide, also known as Perylene Orange (PO), was selected due to its strong absorption in the green region (Figure S1, Supporting Information), and its proven compatibility with liquid crystal (LC) systems.[43] Therefore, a green light-emitting diode (LED) with peak emission at 525 nm was chosen as a light source to stimulate the system. Different percentages of dye have been incorporated as will be detailed later.

2.2. Printing and Photopolymerization Process. Photochemistry Assessment

The LCE actuators were prepared using a printing equipment developed in our group, consisting of a CNC router coupled to a fluid dispenser, as described in the Experimental Section.[23] The ink was extruded through a printhead at 70 °C and deposited on a PVA-coated glass substrate. Lines of the ink were closely printed (200 μm distance) to lead to continuous strips generated by the

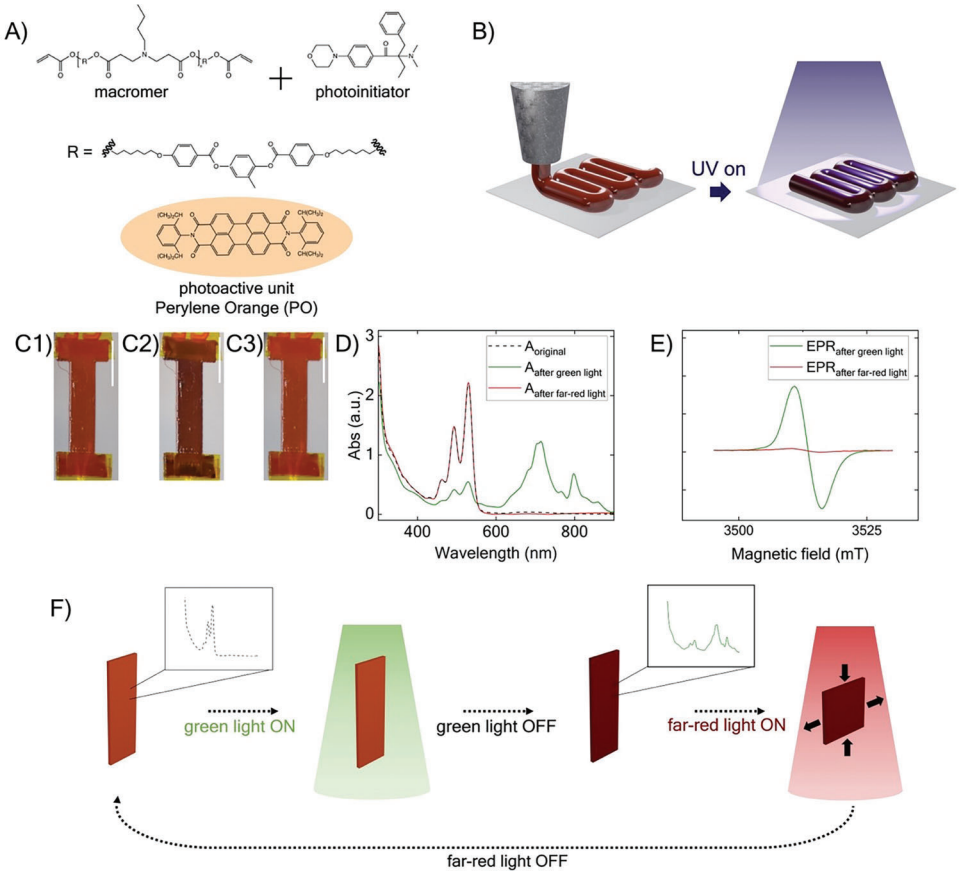

Figure 1. Reconfigurability of 4D printed LCE photoactuators using perylene orange: A) Chemical structure of the ink components including macromer, photoactive unit and photoinitiator. B) Conceptual representation of the printing and photopolymerization process under UV light. C) Color change observed when irradiated with green and, immediately after, with far-red light. Photographs show the change in the color of the actuator after irradiation with light of different wavelengths. The original sample (C1) turns into a dark red when exposed to green light (525 nm, 280 mW cm^{-2}) (C2), and after irradiating with far-red light (740 nm, 450 mW cm^{-2}), it recovers its original orange color (C3). D) Absorption spectra of a 60 µm thick actuator. The black dotted line represents the original spectrum, whilst the continuous green one shows the spectrum of the actuator after being irradiated with green light (525 nm) of 280 mW cm^{-2} for 2 min. The continuous red line represents the spectrum of the actuator after being irradiated with far-red light (740 nm) of 450 mW cm^{-2} for 2 min, immediately after the green light exposure. E) EPR spectra carried out at similar stages as the UV–vis-NIR spectrum. The green EPR signal was the one detected right after the green light exposition, corresponding to the fast-decaying radical species whereas the red one represents the signal detected after being irradiated with far-red light (740 nm) of 450 mW cm^{-2} for 2 min, immediately after the green light exposure. F) Conceptual representation of the reconfiguration process of the material under study. Originally, the LCE actuator is sensitive to green light, showing almost no absorption in the far-red or NIR regions. The irradiation with green light induces the appearance of absorption bands in the far-red and NIR region, making the material sensitive to light in these regions of the electromagnetic spectrum. When the material is irradiated with far-red light, immediately after the green exposure step, the film not only recovers its initial spectrum, but also could modify its dimensions due to the photothermal effect.

fusion of these adjacent lines. As it is now well-known, the shear forces and/or elongational flow during the printing process favor the orientation of the polymeric chain, and therefore of the mesogens, along the movement direction of the needle. This alignment behavior was confirmed in our system for the employed printing conditions, by observing the printed samples using a polarization optical microscope (POM) (Figure S2, Supporting Information). These observations are consistent with previously reported studies, indicating LC director alignment along the printing direction.[23] This phenomenon thus provides digital control of the morphology of the printed material.

Once deposited, the ink is photopolymerized by exposing it to UV light as conceptually shown in Figure 1B, leading to the final LCE that retains the director morphology initially imposed during printing. Gel fraction tests were performed with all the ink batches prepared in this work, obtaining values ≈90%, indicating a good efficiency of the polymeric network formation process.

Remarkably, a color change of the sample, from the original orange to purple, was observed after being exposed to UV light to photopolymerize (Figure S3, Supporting Information). After 24 h at room temperature (RT) and ambient conditions, the sample recovered an orange color which remains stable over time. Previously published studies carried out in systems containing perylene dyes suggest that this color change upon UV irradiation may be associated with a radical formation process in these molecules.[44] For all the experiments presented in this work, the samples were left 24 h in darkness after UV curing so the sample recovered the initial orange color.

Once the perylene-doped LCE elements were prepared, preliminary actuation experiments carried out using green light (525 nm), at the absorption maximum of the PO dye, showed a new color change of the LCE sample, from original orange to a rather dark red, after this irradiation step. Trying to understand the ongoing changes in the material, we have performed UV–vis-NIR spectroscopic studies on LCE samples prior to and after exposure to green light. Inks with 0.5 wt.% dye have been chosen for these initial experiments as they lead to printed LCE samples with optical densities well suited for optical absorption characterization. Prior to irradiation with green light, the sample presents an absorption spectrum that resembles that of the dye in solution, except for a small background absorption in the 600 to 800 nm region (vide infra). Upon illumination with green light of 280 $mWcm^{-2}$ for 30 s, the actuator (60 μm) also experienced a color change toward a dark red (Figures 1C1–C3, Supporting Information). Light absorption characterization of the sample just after its irradiation with green light revealed a significant decrease in the absorption at 530 nm while new absorption bands appeared in the far-red and IR region (Figure 1D). After 30 min in darkness, these new absorption bands strongly decreased and completely disappeared after 24 h. Nevertheless, even though the main peak in the visible region (at 530 nm) retrieved its shape, it did not reach its original height, having a 15% of non-recovery after 30 min of relaxation in darkness, a loss value that remained after 24 h (Figure S4A, Supporting Information).

Notably, in a similar experiment, in which exposure of the actuator to a subsequent far-red light (740 nm) irradiation of 2 min at 450 mW cm^{-2}, is carried out just after green light exposure, a recovery of the band in the green region (within 1%) was observed while the strong far-red and IR bands completely disappeared (Figure 1D). A similar experiment was conducted substituting the far-red light exposure step with a NIR exposure with light coming from a LED with an emission peak at 850 nm, finding that this wavelength also accelerates the recovery of the original orange color of the material.

The results obtained from these spectroscopic experiments were thought to be related to the appearance of radical species previously reported in other works based on green light irradiated perylene molecules.[44–46] To confirm this hypothesis, electron paramagnetic resonance (EPR) studies were conducted. As it can be seen in the EPR spectrum shown in Figure 1E, after green light irradiation a single absorption feature, centered at $\approx g = 2.00$ and ≈0.5 mT broad, was displayed, that is fully compatible with an organic radical species. When studying the time evolution of this feature, a rather fast decay was found. The intensity of this fast-decaying signal can be fitted to a single exponential decay, with a decay constant of ≈19 min. (see Figure S4B, Supporting Information). This decay corresponds to the time scale of the evolution in darkness of the far-red and NIR bands generated by green light, previously described in the absorption experiments (Figure S4A, Supporting Information). Additionally, while the fast-decaying EPR feature decreased, another much weaker and broader (centered at $\approx g = 2.00$ and ≈0.8 mT) EPR feature was revealed. This signal should be associated to a second radical species. It also shows a time decay, with a much longer time constant (≈50 h).

EPR studies were also carried out to elucidate the effect of far-red light on these two radical species, observing that only the fast-decaying radical was sensitive to this wavelength, the effect of which consisted of the complete blurring of its associated EPR signal, revealing that, after far-red light, only the slow-decaying signal was present in the EPR spectrum, shown in Figure 1E. On the other hand, this slow-decaying signal was not affected by the subsequent far-red irradiation, as the observed time evolution was similar with and without far-red light exposure.

As anticipated, the time evolution of the EPR spectrum, and specifically that of the fast-decaying signal, can be correlated with those obtained in the UV–vis-NIR absorption experiments. As it can be seen in Figure 1D, the irradiation with green light decreases the height of the main bands of the absorption spectrum and makes new ones to appear in the far-red and NIR, also causing the emergence of the fast-decaying EPR signal. The immediate exposure with far-red light led to the recovery of the original absorption spectrum as well as to a complete vanishing of this fast-decaying EPR signal.

Concerning the relationship between fast-decaying and slow-decaying EPR signals, it seems clear that both are connected with the green irradiation process. Whether the second one is produced by the first one, or they both have an independent origin, cannot be established from our results. On the other hand, it can be stated that far-red light has no effect on the decrease of the slow-decaying signal. Although the nature and dynamics of the radical species formed are of great interest, their in-depth investigation is out of the scope of this paper in which we focus on the use of the light-induced radicals for the light-induced reconfiguration of our 4D printed LCE actuators.

To evolve toward this reconfiguration concept, we need to be able to transform the system between two different states, unprogrammed and programmed ones. On one hand, the original state of the sample, that we will refer as unprogrammed state, is strongly sensitive to green light, as the incorporated photoactive unit shows a high absorption in the green region. However, it is nearly transparent to far-red and NIR light in this initial state. On the other hand, as it has been demonstrated, the exposure to green light generates the appearance of radical species absorbing in the far-red and NIR regions and, therefore, making the system photothermally responsive to light in these wavelengths of the spectrum. We will refer this as the programmed state. The irradiation of this state with far-red and NIR light, immediately after the green light exposure, not only could trigger the photothermal effect characteristic of LCEs, but also returns the system to its original unprogrammed state. Thus, this approach based on the generation and erasure of a radical species with a two-wavelength light scheme opens the way for a reconfiguration process exclusively based on the use of green and far-red and NIR light sources, in contrast to other strategies that involve the use of UV light (Figure 1F).[37,42]

2.3. Mechanical Response Characterization

2.3.1. Thermal Actuation

After the printing process, and once the spectroscopic characterization of the material was assessed, actuators were tested in terms of their mechanical actuation response. First, and prior to undertaking further photomechanical studies, a mechanical

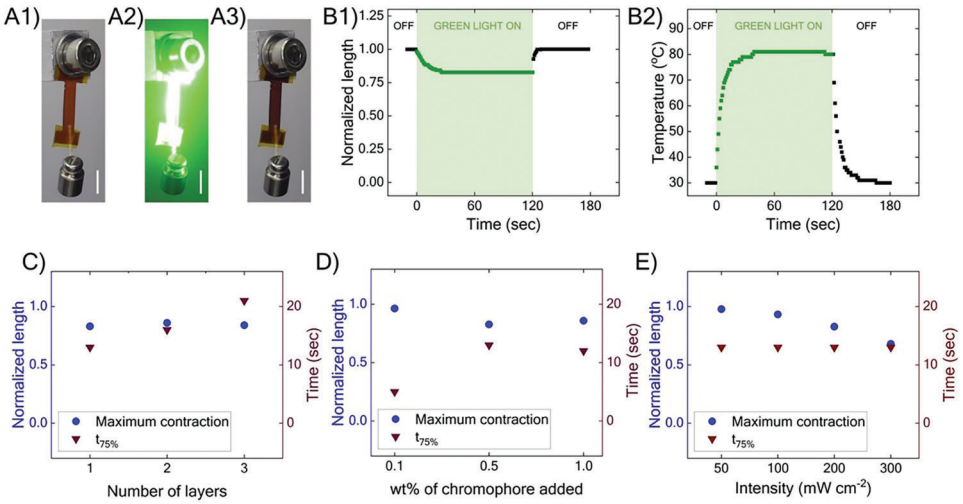

Figure 2. Unprogrammed state: Photoinduced actuation under green light of the PO-LCE. A) Images successively acquired of the LCE actuator before the green light irradiation (A1), after 2 min at 200 mW cm^{-2} (A2) and 1 min after switching off the light source (A3). Scale bar represents 5 mm. B) Photoresponse of a LCE strip (100 µm thick) with uniaxial orientation of the director along the long axis and a 1 g weight attached to its free end, with a green light source of 200 mW cm^{-2}. Temporal dependence of normalized strip length (B1) and temperature (B2), upon green light illumination (green squares) with 200 mW cm^{-2} and the recovery when green light illumination ceases (black squares). C) Thickness dependence of the maximum contraction (blue dots) and the time to reach 75% of the maximum contraction, $t_{75\%}$ (deep red inverted triangles) when irradiating with green light of 200 mW cm^{-2}. D) Maximum contraction (blue dots) and $t_{75\%}$ (deep red inverted triangles) when irradiating with green light of 200 mW cm^{-2} for samples with different concentration of PO. E) Maximum contraction reached (blue dots) and $t_{75\%}$ (deep red inverted triangles) for different green light intensities.

response characterization of the material as a function of temperature was carried out. These experiments were made for the purpose of knowing whether the chromophore molecule affects the mechanical capacity of the sample. To test the reproducibility and repeatability, two thermal cycles were performed on each sample used in this work.

Single-layer uniaxially oriented actuators with the director along its long axis and an average thickness of 100 µm, were then subjected to a thermomechanical test that consisted of a heating process from 30 to 100 °C and a subsequent cool down process back to 30 °C, taking pictures every 5 °C. Figure S5A (Supporting Information) shows the length (L) and width (W) versus temperature normalized by the initial length (L_0) and width (W_0) for a standard single-layer PO-doped LCE actuator when coupled to 1 g weight. This weight is applied to prevent any bending deformation upon irradiation later in subsequent photomechanical experiments. This experimental configuration also allows to better quantify the dimensions changes of the LCE actuators. We note that it was checked that similar thermomechanical deformation, within the experimental error, was measured with unloaded samples indicating that this 1 g load does not limit the thermomechanical performance of our actuators. The material presents a contraction of 37% at 100 °C and recovers its initial length once the temperature is back to 30 °C. This elongation process takes place along with the expansion on the short axis direction of the actuator, reaching 26% of deformation regarding its initial width. The microscopic mechanism behind this phenomenology relates to the increase of the mesogenic disorder, caused by the increment of temperature, that leads to a shortening of the actuator along the director and an expansion along the perpendicular direction, as previously reported.[23,47]

2.3.2. Photo Actuation

Understanding the photothermal actuation of the material under study is one of the main goals of this work. To gain insight into the material's photomechanical behavior, irradiation experiments using different wavelengths, green, far-red and combinations of them, were performed.

Photoinduced Actuation under Green Light. Unprogrammed State: As seen in Figure 1D, the PO-LCE has its main absorption peaks in the green region. The dependence of the photoinduced contraction while green light of 200 mWcm^{-2} is on, in a single-layer actuator doped with 0.5 wt.% of PO, is shown in **Figure 2**. It can be seen how the actuator undergoes a maximum contraction of 17%, reaching 75% of its maximum value (13% of its original length) in 13 s (Figure 2B1). This value of deformation is maintained whilst light is still on. Once the green light is off, the LCE actuator recovers its initial length in a few seconds. In turn, in Figure 2B2, we can observe the evolution of temperature with time associated with the contraction process previously studied, seeing that this contraction takes place along with an increment of temperature of 50 °C, with 80 °C the maximum temperature reached. Likewise, when green light is switched off, the surface temperature of the actuator also shows a fast decay to RT. Thermoactuation studies, previously shown in Figure S5 (Supporting Information), presented a deformation of 16% at 80 °C, results that are consistent with the photoinduced contraction and photoinduced heating measured in this experiment, which indicates that the light-induced deformation has a photothermal origin.

The influence of actuator thickness, dye concentration, as well as the light intensity has been explored for our system. First, the photoresponse to green light of actuators with different

thicknesses, obtained by accumulating layers through additive manufacturing, was assessed. Figure 2C shows the maximum deformation achieved for samples of different thicknesses irradiated with the same dose of green light (200 mW cm^{-2}). Besides, the dynamics of the green light-induced contraction were studied by estimating the time it takes the actuator to reach 75% of its maximum contraction, denoted as $t_{75\%}$, also plotted in Figure 2C. Results show that regardless of the thickness, the final contraction is similar in all the studied samples although the saturation time is faster for the thinner ones. Thermographic characterization of the samples during the irradiation experiments shows that the final temperature achieved is, in all the cases ≈80 °C (Figure S6, Supporting Information), although temperature saturation times in the thickest actuator (300 µm, 3 layers) are longer (see Figure S6, Supporting Information). The longer times to reach maximum contraction and temperature for actuators with an increasing number of layers are related to the increasing mass of these actuators together with the strong absorption of green light (see Figure 1D) in our elements. These present high optical densities in this wavelength range during all the irradiation time, so most of the incident light is being absorbed, for all the studied elements, in the first part of their film thickness. With, essentially, the same amount of energy deposited in all the samples, regardless the number of layers, the larger mass of thicker samples requires more energy and therefore more time to reach the temperature stationary value. Similarly, when the light stimulus ceases, actuators with larger mass also require a longer time to recover their initial temperature value.[48] Considering these results, and seeking for a fast performance of the elements, a single-layer actuator was chosen for all the experiments to continue with the material photoinduced actuation characterization.

The amount of chromophore incorporated into the material was also meaningful when it comes to the performance of the material. For this purpose, different percentages of chromophore ranging from 0.1 to 1 wt.% were added to the LCE precursor ink and the photoresponse of the resultant LCEs studied. Figure 2D shows that reducing the percentage of chromophore led to faster mechanical response of the LCE actuators although to smaller stationary values of deformation, when comparing the behavior observed on actuators doped with different percentages of chromophore while green light irradiation of 200 mW cm^{-2} takes place. The smaller contraction observed in the actuators with lower concentrations of chromophore is understood taking into account that the amount of energy deposited in these films is smaller, as they present lower absorption compared to those having higher chromophore content, while the faster response is associated to the smoother profile of absorption through the film thickness, that allows a less heterogeneous delivery of the energy in the film, leading to a quicker equilibrium of the temperature in the system. On the other hand, similar values of contraction of ≈11–13% are obtained for the samples with 0.5 wt.% of chromophore or higher (1 wt.%). Also, similar photoinduced heating dynamics and saturation temperatures are observed for these two samples, indicating a saturating behavior of the photoresponse with respect chromophore content in these range of concentrations (Figure S7, Supporting Information). Although the light intensity decay in the illuminated side of the films is expected to be sharper in those with higher percentage of chromophore, this difference does not significantly affect the global photomechanical behavior of the film. For this reason, from now on all the tests were performed with PO-LCE doped with a 0.5 wt.%, as they present high values of photodeformation with a lower amount of dye.

The influence of green light intensity has also been studied. With this aim, single-layer actuators were exposed to values of green light intensity between 50 to 300 mW cm^{-2}, as shown in Figure 2E. The irradiation with higher intensities of green light consistently results in higher contraction values, as more energy is being deposited in the actuators, reaching, with 300 mW cm^{-2}, a 32% of contraction along the long axis, with a surface temperature of 96 °C, being these values consistent again with the thermoactuation tests. Similar response times to reach saturation were observed in the irradiated elements for the different intensities studied.

Summarizing this section, the obtained results demonstrate that the control in the thickness and the amount of PO chromophore in the printed elements, together with the employed green light intensity, allows to tailor the actuation response of the actuator in this unprogrammed state.

Photoinduced Actuation under Far-Red Light. Programmed State: The green light-induced generation of radical species described above, leading to significant absorption of our LCE elements in the far-red region of the spectrum, offers the possibility of activating the response of these systems to far-red light. Before exploring the mechanical photoresponse of this, so-called, programmed state, first, we have studied, as a reference experiment, the response of a single-layer actuator in the unprogrammed state (**Figure 3**A1), that is without previous exposition to green light, when exposed to a far-red light source (740 nm) of 675 mW cm^{-2} (Figure 3A2). As shown in Figure 3C1, the unprogrammed actuator reached a maximum contraction of 4% when exposed to far-red light. This slight contraction took place along with an increment of the temperature of the LCE element from RT to 51 °C, which was maintained whilst the far-red light source was on (Figure 3C2). When the far-red light is switched off, the system recovers its initial length in a few seconds reaching also quickly RT. In contrast, we have performed a homologous experiment with an actuator having the same structural configuration (Figure 3B1), but exposed, immediately before, to green light of 200 mW cm^{-2} for 45 s (Figure 3B2). This actuator showed a maximum contraction of 40% of its length in ≈6 s (Figure 3C1), followed by a slower decay, in ≈18 s, to a contraction of 4%, the same value reached by the actuator under far-red light in the unprogrammed state. This fast peak contraction of the programmed actuator took place along with an increment of its temperature up to 116 °C in 6 s, that decayed in turn to 51 °C in the next 18 s (Figure 3C2). The rapid far-red light-induced heating and resulting contraction of the samples may be associated with the absorption of the so-called fast-decaying radical species identified by EPR. These radical species quickly disappear under far-red light irradiation, as shown above, leading to a film with low absorption in this region of the spectrum (see Figure 1D) and thus a relaxation to a length corresponding to the film before the programming step with green light, with little photoinduced heating when exposed to far-red light.

To explore the photoresponse of the LCE material regarding the programming step, different green light illumination schemes of pre-irradiation were applied while keeping the same

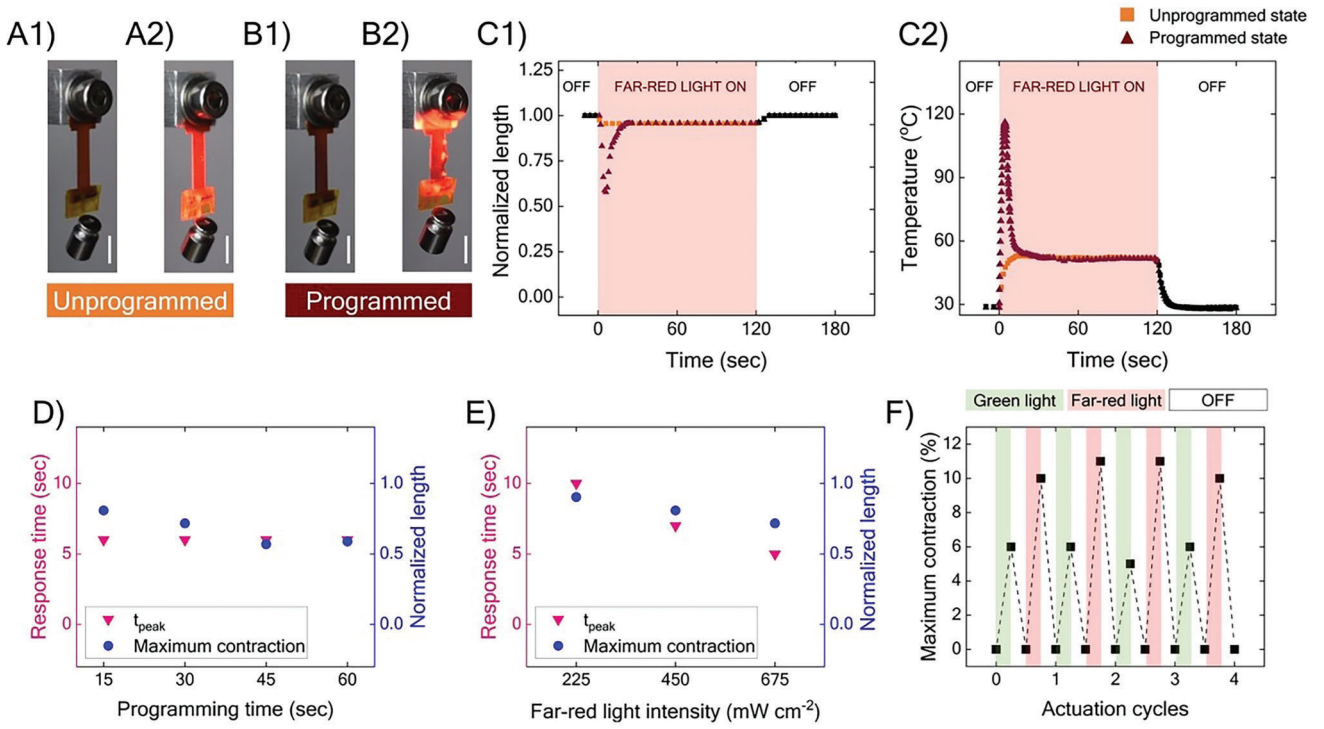

Figure 3. Programmed state: Photoinduced actuation under far-red light of the PO-LCE. A) Images of the LCE actuator acquired just before far-red light illumination (A1) and after 6 s of switching on light source (A2), on their maximum contraction state, for the unprogrammed actuator. B) Images of the LCE actuator acquired just before far-red light illumination (B1) and after 6 s of switching on light source (B2), on their maximum contraction state, for the actuator programmed with 200 mW cm^{-2} of green light for 45 s. Scale bar represents 5 mm. C) Photoresponse under far-red light illumination of a LCE strip (100 µm thick) with uniaxial orientation of the director along the long axis and a 1 g weight attached to its free end, on its unprogrammed state and on its programmed state with green light irradiation of 200 mW cm^{-2} for 30 s. C1) Temporal dependence of the normalized strip length upon far-red illumination with 675 mW cm^{-2} of an unprogrammed (orange squares) and a programmed element (deep red triangles). The sample recovers its original length when far-red illumination ceases in both, the unprogrammed (black squares) and the programmed state (black triangles). C2) Time evolution of the sample temperature upon far-red illumination with 675 mW cm^{-2} of an unprogrammed (orange squares) and a programmed element (deep red triangles). The sample temperature relaxes to RT when far-red illumination ceases in both, the unprogrammed (black squares) and the programmed state (black triangles). D) Peak temperature time (t_{peak}, pink inverted triangles) and maximum contraction values (blue dots) reached upon far-red light irradiation (at 675 mW cm^{-2}) on a single layer actuator (100 µm) for different green light (200 mWcm^{-2}) programming times. E) Peak temperature times (t_{peak}, pink inverted triangles) and maximum contraction (blue dots) upon irradiation with different far-red light intensities. F) Assessment of the reproducibility and repeatability of the experiments in terms of contraction of the material. A LCE strip (100 µm thick) with uniaxial orientation of the director along the long axis of the element and with a weight of 1 g attached to its lower extreme was exposed to a 4-step irradiation cycle. Each cycle consisted of the following sequence of four steps: i) 30 s of green light irradiation at 200 mW cm^{-2}, ii) 30 s without exposure, iii) 60 seconds of far-red light irradiation at 300 mW cm^{-2}, and iv) 30s without exposure.

intensity of far-red light. First, we have maintained the green light pre-irradiation intensity at 200 mW cm^{-2} but have varied its irradiation time. After 60 s in the dark, the sample is irradiated with a fixed intensity of far-red light (675 mW cm^{-2}). Figure 3D shows the maximum contraction and peak temperature time (t_{peak}) reached. It can be seen how this peak time reached with far-red light was a nearly constant value of ≈6 s, regardless of the previous green light pre-exposure time. However, the maximum temperature reached, and consequently, the induced contraction was different and consistent with the previous results obtained: the longer the exposure to green light is, the higher contraction obtained with far-red light, which is ascribed to the presence of more far-red absorbing species for samples irradiated longer with green light (Figure S8, Supporting Information).

Once the influence of the green light pre-irradiation step has been explored, to strike a balance between a sufficient contraction with a short duration of the green light exposure, the programming conditions, for subsequent experiments, were selected as 200 mW cm^{-2} of green light for 30 s. As in the previous set of experiments, 60 s after the green light irradiation step, different light schemes of far-red light were tested, leading to different peak contractions as well as different times to reach these peak contraction values.

As it can be seen in Figure 3E, a higher intensity of far-red light drove to a faster and more pronounced contraction, reaching a value of 28% of its initial length when exposed to 675 mW cm^{-2} in ≈5 s. After the peak contraction, the system evolves toward a stationary contraction corresponding to the unprogrammed actuator. This phenomenology is consistent with the model presented before consisting of green light-induced radical species that decay back to the original state under far-red irradiation.

To test the repeatability of the programming and actuation steps, several cycles consisting of irradiation with green light (programming) followed by irradiation with far-red light

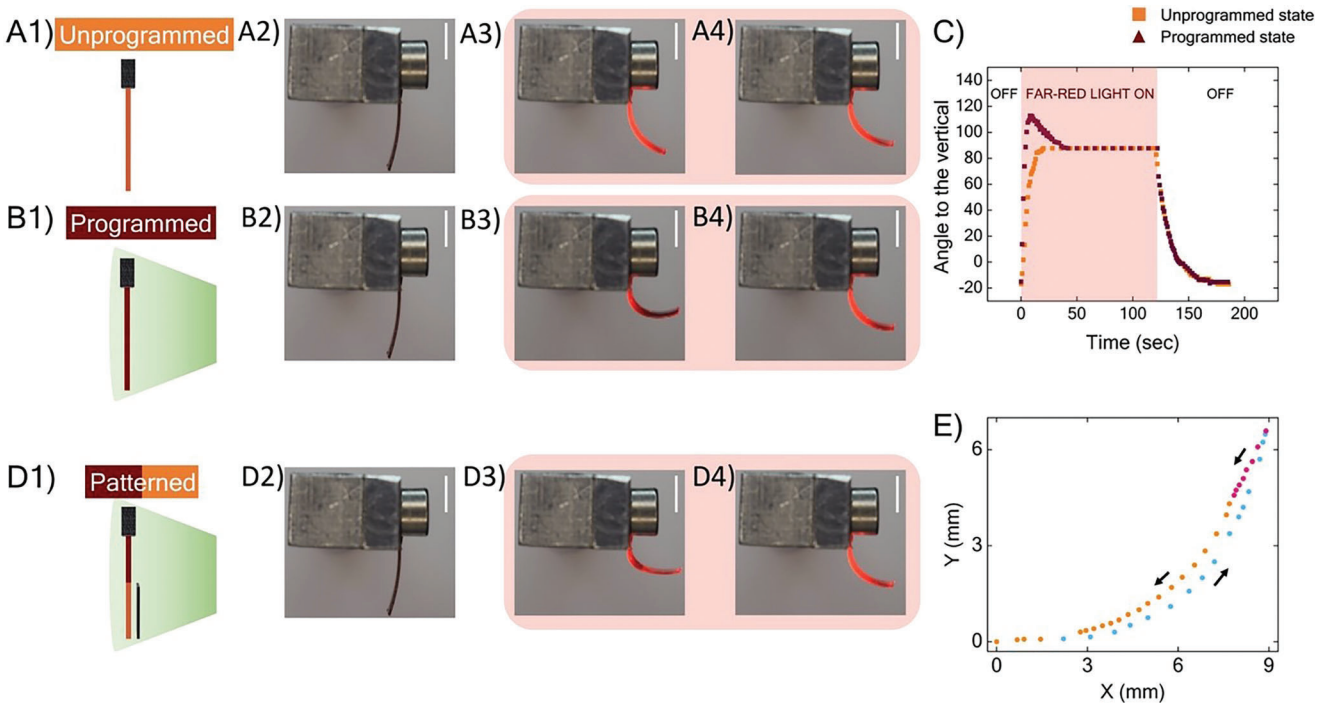

Figure 4. Reconfigurability of 4D printed LCE bimorph actuators: A) Performance of an unprogrammed 4D printed LCE bimorph actuator under far-red light. A1) Conceptual representation of an unprogrammed bimorph actuator. Images of the unprogrammed LCE actuator acquired before far-red light irradiation (A2), 10 s after switching on the far-red light (A3) and 50 s after switching on the far-red light (A4). Scale bar represents 5 mm. B) Reconfigurability of a 4D printed LCE bimorph actuator (previously programmed) under far-red light. B1) Conceptual representation of a programmed bimorph actuator. The actuator is first irradiated with green light of 200 mW cm^{-2} for 30 s. Once green light is switched off, the actuator is left to recover its original configuration. Images of the programmed LCE actuator acquired before far-red light irradiation (B2), 10 s after switching on the far-red light (B3) and 50 s after switching on the far-red light (B4). Scale bar represents 5 mm. C) Angle to the vertical described by the 10% of the length of the actuator over time in the cases described in A) and B). The angle is measured with respect to the vertical, the clockwise direction being negative and the counterclockwise direction positive. D) Reconfigurability of a 4D printed LCE bimorph actuator (previously partially patterned) under far-red light. D1) Conceptual representation of the green light patterned LCE actuator proposed as a proof of concept of the programming strategy developed. The half of the actuator far from the fixing extreme is covered with a dark mask that prevents the sample from being exposed to green light and therefore, from becoming more far-red light sensitive. Upon far-red light irradiation, the LCE actuator bends with different grades of folding in its two halves, reaches a bending equilibrium state whilst far-red light is still on and goes back to its initial configuration once the far-red light is switched off. Images of the programmed LCE actuator acquired before far-red light irradiation (D2), 10 s after switching on the far-red light (D3) and 50 s after switching on the far-red light (D4). Scale bar represents 5 mm. E) Coordinates in the x-y plane of the free extreme of the actuator. The area determined by the bending and unbending graphs revealed that the actuator describes a non-reciprocal motion.

(actuation) were carried out, with comparable results in terms of light-induced contraction after 4 cycles (see Figure 3F).

Reconfigurable Photoresponse of 4D Printed LCE Actuators: We aim to demonstrate that these light reconfigurable actuators can be programmed, by using patterned green light, to later reproduce different complex deformation modes by exciting the element with a single and homogeneous light source in the far-red, without the need for any structural modification of the actuator or any additional light source. To explore the possibilities of this reconfiguration strategy, we have used, as a first example, a bimorph actuator consisting of a 4-layered LCE rectangular element with dimensions 12 × 3 mm (L x W), with pairs of layers printed in two different orthogonal directions (along the long side of the rectangle and perpendicular to it) as shown in Figure S9 (Supporting Information). It is well known that this type of bimorph actuator leads to bending when LC disorder is generated upon stimulation.[49] When the actuator is exposed to a stimulus, for example heat, the first two layers, printed along the long axis, tend to contract themselves along this direction, while the upper layers, printed along the short axis of the rectangular actuator, contract themselves along this short direction and expand along the orthogonal directions. As a result, to accommodate these stimulus-triggered stresses, the strip bends outside the plane. As a first reference experiment with this bimorph-type actuator, this was exposed to far-red light for 2 min without any pre-irradiation with green light, that is in the unprogrammed state. As seen in **Figure 4**A, upon far-red light irradiation (450 mW cm^{-2}), the actuator progressively bends until it reaches, after 15 s, a maximum deformation curvature that is kept constant until light is switched off, completing a 2-minute irradiation period (see Figure 4A2–A4; Movie S1, Supporting Information). After light is switched off, the bimorph progressively recovers the initial state in ≈40 s. After this first reference experiment, with no green light programming, a second reference experiment, this time with green light pre-irradiation (200 mW cm^{-2} for 30 s), was carried out to explore the actuation of the programmed state (conceptually shown in Figure 4B1). The whole actuator changes its color to deep red, upon green light exposure, indicating the

generation of the far-red light-absorbing radicals. The so-programmed actuator was subsequently irradiated with far-red light for 2 min (450 mW cm^{-2}). A faster and more pronounced bending is initially observed in this case, with respect to the previous experiment in which the actuator was unprogrammed. A maximum deformation is achieved in ≈10 s and after this moment the system progresses, in ≈30 s while under constant far-red irradiation, to the bending state equivalent to the non-programmed one, keeping it that way while the far-red light is on (see Figure 4B2–B4; Movie S2, Supporting Information). Once the far-red light is switched off, the actuator recovers its original state.

To quantify and better compare the results of these two reference experiments, Figure 4C shows the angle forming the tip of the actuator (the terminal 10% length of the actuator) with the vertical direction. Although both actuation modes converge to the same bending angle at the end of the far-red irradiation step, they follow significantly different dynamics at the early stage of the illumination. The observed results can be explained in terms of the photoinduced heating of the sample, and the presence of green light-induced radicals. As in previous photoinduced contraction experiments, shown in Figure 3C, irradiation with far-red light of the unprogrammed samples induces limited photoinduced heating. Differently, green light programming induces radical species, that absorb light in the far-red leading to photothermal actuation, upon illumination in this wavelength range. As far-red light irradiation proceeds, the radicals disappear and therefore absorption of the system converges back to that of the unprogrammed actuator, reaching the system the same photoinduced heating and thus the same photodeformation final state.

After these reference experiments, we aim to gain advantage of this programming strategy by introducing a green light pattern to create regions with different folding abilities. Our aim is to introduce, through this patterning, different dynamic behaviors in different parts of the bending actuator that could lead to a non-reciprocal movement while using one single and homogeneous light source for actuation in the far-red region of the spectrum. For this purpose, a mask was placed to cover the half of the sample corresponding to the free end of the actuator, protecting it from the green light, while the other half, the one close to the fixing extreme, is uncovered, being therefore exposed to the green light, as schematically shown in Figure 4D1. In this programming configuration, exposure of the sample through this mask to green light (30 s at 200 mW cm^{-2}) induced a change in color in the exposed region, the half of the actuator close to the fixing extreme, indicating the formation of radicals in this area, while the other region remains unchanged. Just after finishing the green light irradiation, the mask was removed, and the entire actuator was immediately irradiated with homogeneous far-red light (450 mW cm^{-2}). The actuator starts to bend but the two halves, unprogrammed and programmed, follow different dynamics. A faster and more pronounced bending is appreciated for the green light programmed half of the actuator compared to the other half. After a few seconds, in which the programmed half has reached the maximum bending, this progressively evolves toward a less pronounced curvature. The unprogrammed half, on the other hand, progressively evolves to its maximum curvature at a slower pace. After 30 s, both halves have reached their equilibrium situation under far-red light (see Figure 4D2–D4; Movie S3, Supporting Information). When light is switched off, the system relaxes back to the initial configuration. Figure 4E presents the coordinates in the x-y plane of the free extreme described by the actuator. The extreme of the actuator does not follow the same path when progressing toward the maximum bending when compared to the unbending stages. The bending and unbending paths determine a measurable area, a feature known as non-reciprocal motion, that is a motion exhibiting time-reversal asymmetry as those found in many natural species to attain locomotion.[50]

More complex shape morphing modes can be undertaken by combining the capability of our printing platform to digitally define complex director patterns together with the programming capabilities of the presented PO-LCE system using patterned irradiation. **Figure 5**A shows the conceptual representation of an actuator with a spiral-like configuration of the director. This actuator is known to morph, under homogeneous stimulation, into a conical shape as predicted by Warner and coworkers.[15,16,23] This morphing paradigm is clearly observed when an unprogrammed sample, with this director configuration, is irradiated with homogeneous far-red light. Figure 5B shows the formation of a cone upon irradiation with the apex at the center of the disk. An increase of the disorder, produced by photoinduced heating of this system, leads to a contraction along the spiral direction and an expansion along the radial one. To accommodate the stresses the flat actuator escapes the plane turning into a conical shape.

Besides the complex conical shape morphing dictated by the director pattern, we can reconfigure this actuator into a different shape morphing geometry by exposing it to green light through a mask. Following the circular symmetry of our sample we have used a dark annular mask leaving the central part of the spiral uncovered, as seen in Figure 5C. Irradiation of the sample with green light through this mask induces radicals in the exposed central area making this region more sensitive to far-red light, while the outer annular region of the sample remains less sensitized to the far-red light. Irradiation of this, so reconfigured sample with far-red light, leads to the fast emergence of a cone in the central region, as seen in Figure 5D and Movie S4 (Supporting Information), while the outer annular region, morphs making undulations along the azimuthal direction. Overall, the flat disk morphs to a "witch hat" shape after 10 s of far-red light irradiation. The undulations in the outer annular region resemble that of the anticones predicted by Warner and co-workers for azimuthal director profiles on cooling, in which the system tends to increase the circumference while decreasing the radius leading to a surface that azimuthally oscillates.[15] As far-red light irradiation progresses; the amplitude of the undulations decreases until it vanishes, and the entire sample adopts a well-defined conical shape. The observed behavior can be understood considering the inhomogeneous heating of the sample during the far-red light irradiation step. The temperature in the central programmed region quickly increases upon far-red light irradiation, leading to the central emerging cone, while heating is slower in the outer annular part. We hypothesize that the strong conical deformation of the central region can stress the annular part of the sample trying to diminish its circumference beyond the length naturally corresponding to the temperature achieved in this annular region. At this stage of the irradiation, this annular region, being "too long" for the inner cone circumference, accommodates

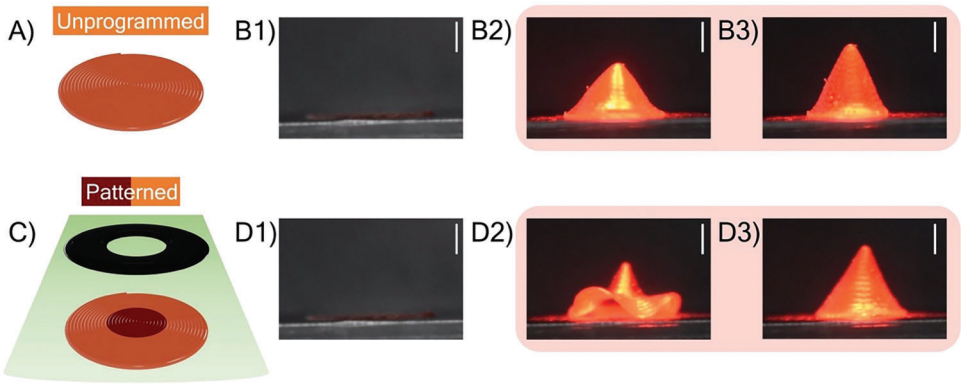

Figure 5. Reconfigurability of 4D printed LCE spiral actuators: A) Conceptual representation of an unprogrammed actuator with a spiral-like configuration of the director. B) Behavior of a spiral-like unprogrammed LCE actuator under far-red light. Images before far-red light is switched on, when the actuator remains flat (B1), once the light is switched on, the cone starts to appear (picture taken at 10 s), (B2) and after 50 s, forming a well-defined cone (B3). C) Conceptual representation of an actuator with a spiral-like configuration of the director, with an annular dark mask centered on top of the sample used for the patterning step. Upon green light irradiation (200 mW cm^{-2} for 30 s) through the dark annular mask, the central circular region of the sample becomes sensitized to the far-red light while the outer ring remains unsensitized. D) Behavior observed on the actuator with a spiral shape under far-red light immediately after the green light patterning step. Images before far-red light is switched on, the actuator being flat (D1), once the light is switched on, the cone emerges in the central region while there are azimuthal undulations in the outer ring (picture taken at 10 s), overall the sample morphing into a "witch hat" shape (D2), and after 50 s, a well-defined cone is finally formed (D3). Scale bar represents 5 mm.

the stresses by making the observed azimuthal oscillations. As irradiation goes on, the fast-decaying radicals disappear, and the temperature of the sample homogenizes leading to the conical equilibrium shape.

3. Conclusions

We have developed a printable formulation to prepare green to far-red light-driven LCE actuators that can be reconfigured with light to access a plurality of shape-morphing modes. The ink incorporates a dispersed perylene diimide chromophore absorbing in the green region of the spectrum. The resultant LCE elements actuate when exposed to green light throughout a photothermal mechanism, but this exposure process itself also induces the appearance of absorption in the material in the far-red and NIR regions that have been associated with the formation of radical species. These new bands open the possibility to photoinduce mechanical actuation of the element by irradiating at these wavelengths. Advantageously, irradiation of the actuators in these regions of the spectrum immediately after the green light exposure, leads to a recovery of the original absorption spectrum of the actuator. This reversible photoinduced transformation of the LCE elements between two different absorbing states allows to spatially program with green light the actuator in its response to far-red and NIR light, giving access to reconfigurable and reusable soft actuators. By combining the ability of direct ink writing to digitally define the director, together with the possibility to reconfigure the actuation via the programming with green light, complex non-reciprocal morphing paradigms have been demonstrated by using one single, homogenous far-red light source for excitation. The use of the visible to NIR regions of the electromagnetic spectrum, less harmful than UV light, represents an important advantage of our material strategy for various applications of LCEs. The development of homologous materials based on perylene chromophores and LCE matrices with a thermal response at temperatures closer to body temperature makes possible a future scenario in which these smart materials could be applied in the field of biomedicine. We envision their use, as mechanobiological platforms for cell culture, in which these actuators, through suitable stimulation, could apply physiologically relevant strains to cells, effectively emulating, for example, the characteristic peristalsis of the digestive tract organs, or the beating of the heart. In addition to this, their soft nature would also allow their use as actuators in robotic tools in minimally invasive surgery devices. All of these are topics fall within the scope of the planned activities in our laboratory.

4. Experimental Section

Materials: Mesogenic diacrylate 1,4-bis-[4-(6-acryloyloxyhexyloxy) benzoloxy]−2-methylbenzene (RM82, ≥97%) was purchased from Synthon Chemicals GmbH. Chain extender *n*-butylamine (≥99.5%) and solvent tetrahydrofuran (THF, ≥99.9%) were obtained from Merck. The UV photoinitiator 2-benzyl-2-(dimethylamino)−4′-morpholinobutyrophenone (Irgacure369, ≥97%) was acquired from Merck. The visible region absorbing dye N, N′-Bis(2,6-diisopropylphenyl)−3,4,9,10-perylenetetracarboxylic Diimide, also known as Perylene Orange (≥98%), was purchased from TCI Europe N.V. All molecules were used as received. The sacrificial support layer to release the LCE elements was made of polyvinyl alcohol (PVA; 80% hydrolyzed; Mw of 9000-10000) that was purchased from Aldrich.

LCE Precursor Ink Preparation: To begin with, a precursor mixture of a thermoresponsive LCE was prepared using a synthetic procedure published elsewhere.[23] To this aim, n-butylamine and RM82 were added to an amber glass flask with a 1:1.02 molar ratio. Stoichiometry was chosen for the sake of obtaining a material with sufficient crosslinking leading to a good mechanical performance at not too high temperatures of actuation. The mixtures were prepared by adding the photoinitiator (IRG369) in a 1 wt.% ratio. To prepare the precursor mixture of the photoresponsive LCE, Perylene Orange, a perylene diimide, was chosen as photoactive unit. This was added in different percentages from 0.1 to 1 wt.% to explore its effect. Additional THF solvent was added to the flask to obtain a 1:1 weight ratio between THF and the rest of the components. The solution was then made to react for 30 min at 70 °C in a closed flask by using a magnetic stirrer.

Hereafter, the flask was opened and left to stir at 70 °C for 24 h to evaporate THF. Subsequently, the flask is submitted to a vacuum process at 70 °C for additional 24 h to remove the solvent residual fraction and lead to the final photopolymerizable ink. A final checking process was carried out by comparing the weight of the chemicals employed initially and that of the final ink to verify that the level of residual solvent is lower than 1 wt.% (referred to as the weight of THF initially employed).

Printing Equipment: The manufacturing of photoresponsive elements was prepared using a homebuilt 3D printer as beforehand described.[23] The printer is composed of a computer numerical control (CNC) router chassis coupled with a temperature-controlled reservoir for the ink. The pressure was applied on-demand to the reservoir to extrude the ink through the needle while describing X, Y, and Z motions. The printing process is controlled by WinPC-NC software. Computer-aided design (CAD) files were plotted using AutoCAD software. A 10 × 3 mm dog-bone-shaped actuator was created with the preferential orientation of the director, defined by the control of the printing direction, aligned with the long axis of the sample, for the characterization of the material. A 4-layer actuator with dimensions 12 × 3 mm (L x W), was created with the preferred orientation of the director, defined by the print direction control, aligned with the long axis of the sample, in two of its adjacent layers, while the remaining two have an orientation orthogonal to these. Besides, a spiral-like actuator with a diameter of 10 mm was also manufactured. Printing parameters, such as pressure, temperature, speed and distance between substrate and nozzle were optimized for each batch of photopolymerizable ink.

4D Printing of LCE Elements: Printing of elements was carried out on top of conventional glass microscope slides, previously coated with a thin layer of PVA with a thickness of 150 nm. To this end, the glasses were first cleaned by ozone treatment and then coated by spin-coating (1800 rpm for 60 s) with a 5 wt.% PVA solution in Milli-Q purified water. The PVA coating is fixed by drying the solution at 60 °C for 60 min. The material was extruded through a 23-gauge needle tip, with an inner diameter of 330 µm, from a light-protected syringe placed in the temperature-controlled reservoir of the printer previously described. The system was heated to 70 °C, while the substrate was kept at RT. After the printing of one layer, the deposited material was exposed to UV light to trigger photopolymerization (vide infra). Besides single layer, multilayer actuators were printed to evaluate the effect of the thickness and the director profile in the photoresponse of the material. Printing of successive layers was done following the same protocol but raising the printhead a fixed height for each successive layer (typical height step of 80 µm). After each layer the UV curing protocol described below was carried out.

Photopolymerization: Following the printing of a layer, the photopolymerization process was carried out by using a UV lamp from Oriel (Model #6286) and a UV reflecting filter (350-450 nm, Model #66 218). The sample positioned 45 cm from the lamp exit, initially received a light intensity of 30 mW cm^{-2} for 2 min in ambient conditions. Immediately after, each side of the sample was sequentially irradiated for 12 min in a vacuum oven under a mild vacuum of 100 mbar at RT. Once the photocuring step of one layer was completed, successive layers were printed, and the curing was carried out following the same protocol.

Photopolymerization Yield: To calculate the percentage of photopolymerized material, a gel fraction test was performed. For this purpose, the samples were printed and photopolymerized in PVA-coated substrates of known weight, enabling to obtain the initial weight of the actuator (w_i). The samples were then immersed in the solvent, THF, for 24 h. The samples were removed from the solvent and heated for 4 h at 70 °C in a vacuum chamber (100 mbar) to dry them. The samples were then weighed again (w_f) and GF was estimated from the Equation 1:

$$GF(\%) = \frac{w_f}{w_i} \times 100 \quad (1)$$

Polarization Optical Microscopy (POM): To check the molecular alignment of the actuators, LCE were examined using a polarized optical microscope (Nikon Eclipse 80i).

Thickness Characterization: Thickness measurements of the actuators were performed using a profilometer (Bruker DektakXT Stylus Profiler).

Spectroscopic Characterization: Absorption spectra of the samples were taken using a UV-Visible-NIR spectrophotometer (UV–vis-NIR spectrophotometer Cary500, Agilent Technologies).

EPR Characterization: An ELEXSYS E580e EPR spectrometer (Bruker), operating at X band (microwave frequency ca. 9.8 GHz) were used for taking the EPR spectra.

Actuation: After extrusion and photopolymerization of the samples, they were immersed in water to release them from the substrate by dissolving the PVA layer of the glass substrate. The samples were then dried by fixing them to a Kapton tape and letting them in ambient conditions for some hours.

For the thermal actuation characterization, a home-built heated aluminum chamber was used.[51] The chamber is provided with two windows of a cyclic olefin polymer (COP) through which it is possible to obtain optical images. Besides, in one of these windows, there was a hole that allowed the registration of the surface temperature of the actuator by using a thermal camera Gobi from Xenics. A load of 1 g was fixed to the end of the sample, which was then heated from RT to 100 °C with a rate of 5 °C min^{-1}. This heating rate was chosen based on the group's previous experience in this type of experiments, since it is a slow rhythm that allows homogeneity and stabilization of the actuator's temperature.[23,47] Pictures were acquired with a digital camera Nikon D3300. These images enabled to obtain the length and width of the samples at each temperature value. Both dimensions were measured by drawing a parallel line to the long axis of the strip for the former and a parallel line to the short axis of the strip for the latter in Fiji. These values were then normalized by dividing them by the initial values for each sample and experiment.

For the photoactuation characterization of the samples, the actuators were exposed to light coming from a green LED (Thorlabs, central wavelength of 525 nm) or a far-red LED (Thorlabs, central wavelength of 740 nm). Different light intensities were used in the range of 50 to 700 mW cm^{-2}. Weight-lifting experiments were conducted following a homologous method as in the thermoactuation tests, by fixing the samples to a holder and attaching them to a load of 1 g on the other end (Figure S10, Supporting Information). The actuation was monitored by acquiring a video with a digital camera and extracting sample pictures at different moments. The image analysis to obtain sample dimensions as a function of time was performed as previously described for thermoactuation tests. In addition, the surface temperature of the actuators was also measured with the thermal camera to establish the correlation between temperature and mechanical actuation.

Reconfigurability Experiments: A bimorph actuator was also manufactured with 4-layers with dimensions 12 × 3 mm (L x W) and thickness of 240 µm. The first two layers of the actuator were printed aligned with the long axis of the sample, whilst the remaining were printed in the orthogonal direction to the former. Besides, a spiral-like actuator of 10 mm of diameter and three layers (thickness 180 µm) was also prepared for this purpose.

Supporting Information

Supporting Information is available from the Wiley Online Library or from the author.

Acknowledgements

The described research is part of the project PRIME. This project had received funding from the European Union's Horizon 2020 research and innovation programme under Grant Agreement No 829010 (PRIME). Funding had also been received from Spanish "Ministerio de Ciencia, Innovación y Universidades (MCIU)" through AEI/FEDER(UE) PID2020-118485RB-I00 and PID2022-140923NB-C21 projects, Gobierno de Aragón project LMP221_21, FEDER (EU) and Fondo Social Europeo (DGA E15_20R and E09_23R). This research was also supported by CIBER-Consorcio Centro de Investigación Biomédica en Red- (CB06/01/00263), Instituto de Salud Carlos III, Ministerio de Ciencia e Innovación. L.M acknowledges Gobierno de Aragón for a predoctoral fellowship (2020-2024).

C.S.S. acknowledges FAB3D interdisciplinary platform (PTI-CSIC) for support. The authors acknowledge support of the publication fee by the CSIC Open Access Publication Support Initiative through its Unit of Information Resources for Research (URICI).

Conflict of Interest

The authors declare no conflict of interest.

Data availability Statement

The data that supports the findings of this study are openly available in Zenodo at https://zenodo.org/communities/project-prime.

Keywords

4D printing, liquid crystal elastomers, photoinduced radical, reconfigurability, soft robotics

Received: August 1, 2023
Revised: October 4, 2023
Published online: October 20, 2023

[1] B. Mazzolai, A. Mondini, E. Del Dottore, L. Margheri, F. Carpi, K. Suzumori, M. Cianchetti, T. Speck, S. K. Smoukov, I. Burgert, T. Keplinger, G. D. F. Siqueira, F. Vanneste, O. Goury, C. Duriez, T. Nanayakkara, B. Vanderborght, J. Brancart, S. Terryn, S. I. Rich, R. Liu, K. Fukuda, T. Someya, M. Calisti, C. Laschi, W. Sun, G. Wang, L. Wen, R. Baines, S. K. Patiballa, et al., *Multifunct. Mater.* **2022**, *5*, 032001.
[2] B. Mazzolai, C. Laschi, *Sci. Robot.* **2020**, *5*, eaba6893.
[3] S. Palagi, P. Fischer, *Nat. Rev. Mater.* **2018**, *3*, 113.
[4] M. Calisti, G. Picardi, C. Laschi, *J. R. Soc. Interface* **2017**, *14*, 20170101.
[5] Y.-Y. Xiao, Z.-C. Jiang, Y. Zhao, *Adv. Intell. Syst.* **2020**, *2*, 2000148.
[6] M. Pilz Da Cunha, Y. Foelen, R. J. H. Van Raak, J. N. Murphy, T. A. P. Engels, M. G. Debije, A. P. H. J. Schenning, *Adv. Opt. Mater.* **2019**, *7*, 1801643.
[7] H. Zeng, P. Wasylczyk, D. S. Wiersma, A. Priimagi, *Adv. Mater.* **2018**, *30*, 1703554.
[8] A. H. Gelebart, D. Jan Mulder, M. Varga, A. Konya, G. Vantomme, E. W. Meijer, R. L. B. Selinger, D. J. Broer, *Nature* **2017**, *546*, 632.
[9] H. Zeng, O. M. Wani, P. Wasylczyk, R. Kaczmarek, A. Priimagi, *Adv. Mater.* **2017**, *29*, 1701814.
[10] D. J. Broer, J. Broer, *Adv. Mater.* **2020**, *32*, 1905144.
[11] S. Ma, X. Li, S. Huang, J. Hu, H. Yu, *Angew. Chem., Int. Ed.* **2019**, *58*, 2655.
[12] M. Warner, *Annu. Rev. Condens. Matter Phys.* **2020**, *11*, 125.
[13] D. J. Broer, G. N. Mol, *Polym. Eng. Sci.* **1991**, *31*, 625.
[14] H. Yu, T. Ikeda, *Adv. Mater.* **2011**, *23*, 2149.
[15] C. D. Modes, K. Bhattacharya, M. Warner, *Phys. Rev. E* **2010**, *81*, 060701.
[16] L. T. de Haan, C. Sánchez-Somolinos, C. M. W. Bastiaansen, A. P. H. J. Schenning, D. J. Broer, *Angew. Chem., Int. Ed.* **2012**, *51*, 12469.
[17] M. E. Mcconney, A. Martinez, V. P. Tondiglia, K. M. Lee, D. Langley, I. I. Smalyukh, T. J. White, *Adv. Mater.* **2013**, *25*, 5880.
[18] L. T. De Haan, V. Gimenez-Pinto, A. Konya, T.-S. Nguyen, J. M. N. Verjans, C. Sánchez-Somolinos, J. V. Selinger, R. L. B. Selinger, D. J. Broer, A. P. H. J. Schenning, *Adv. Funct. Mater.* **2014**, *24*, 1251.
[19] T. H. Ware, M. E. Mcconney, J. J. Wie, V. P. Tondiglia, T. J. White, *Science* **2015**, *347*, 982.
[20] C. D. Modes, M. Warner, C. Sánchez-Somolinos, L. T. De Haan, D. Broer, *Phys. Rev. E* **2012**, *86*, 060701.
[21] K. M. Herbert, H. E. Fowler, J. M. Mccracken, K. R. Schlafmann, J. A. Koch, T. J. White, *Nat. Rev. Mater.* **2022**, *7*, 23.
[22] C. P. Ambulo, J. J. Burroughs, J. M. Boothby, H. Kim, M. R. Shankar, T. H. Ware, *ACS Appl. Mater. Interfaces* **2017**, *9*, 37332.
[23] M. López-Valdeolivas, D. Liu, D. J. Broer, C. Sánchez-Somolinos, *Macromol. Rapid Commun.* **2018**, *39*, 1700710.
[24] A. Kotikian, R. L. Truby, J. W. Boley, T. J. White, J. A. Lewis, *Adv. Mater.* **2018**, *30*, 1706164.
[25] M. Javadzadeh, J. Del Barrio, C. Sánchez-Somolinos, *Adv. Mater.* **2023**, *35*, 2209244.
[26] Z. Pei, Y. Yang, Q. Chen, E. M. Terentjev, Y. Wei, Y. Ji, *Nat. Mater.* **2014**, *13*, 36.
[27] L. T. De Haan, J. M. N. Verjans, D. J. Broer, C. W. M. Bastiaansen, A. P. H. J. Schenning, *J. Am. Chem. Soc.* **2014**, *136*, 10585.
[28] T. Ube, K. Kawasaki, T. Ikeda, *Adv. Mater.* **2016**, *28*, 8212.
[29] Z. Wang, H. Tian, Q. He, S. Cai, *ACS Appl. Mater. Interfaces* **2017**, *9*, 33119.
[30] M. K. Mcbride, M. Hendrikx, D. Liu, B. T. Worrell, D. J. Broer, C. N. Bowman, *Adv. Mater.* **2017**, *29*, 1606509.
[31] A. H. Gelebart, D. J. Mulder, G. Vantomme, A. P. H. J. Schenning, D. J. Broer, *Angew. Chem., Int. Ed.* **2017**, *56*, 13436.
[32] X. Qian, Q. Chen, Y. Yang, Y. Xu, Z. Li, Z. Wang, Y. Wu, Y. Wei, Y. Ji, *Adv. Mater.* **2018**, *30*, 1801103.
[33] T. S. Hebner, B. E. Kirkpatrick, K. S. Anseth, C. N. Bowman, T. J. White, *Adv. Sci.* **2022**, *9*, 2204003.
[34] E. C. Davidson, A. Kotikian, S. Li, J. Aizenberg, J. A. Lewis, *Adv. Mater.* **2020**, *32*, 1905682.
[35] W. Szymanski, J. M. Beierle, H. A. V. Kistemaker, W. A. Velema, B. L. Feringa, *Chem. Rev.* **2013**, *113*, 6114.
[36] J. Del Barrio, C. Sánchez-Somolinos, *Adv. Opt. Mater.* **2019**, *7*, 1900598.
[37] M. Lahikainen, H. Zeng, A. Priimagi, *Nat. Commun.* **2018**, *9*, 4148.
[38] J. Moan, M. J. Peak, *J. Photochem. Photobiol. B* **1989**, *4*, 21.
[39] K. Kumar, C. Knie, D. Bléger, M. A. Peletier, H. Friedrich, S. Hecht, D. J. Broer, M. G. Debije, A. P. H. J. Schenning, *Nat. Commun.* **2016**, *7*, 11975.
[40] A. Leistner, S. Kirchner, J. Karcher, T. Bantle, M. L. Schulte, P. Gödtel, C. Fengler, Z. L. Pianowski, *Chem. – Eur. J.* **2021**, *27*, 8094.
[41] C. Li, G. Chen, Y. Zhang, F. Wu, Q. Wang, *J. Am. Chem. Soc.* **2020**, *142*, 14789.
[42] K. Kuntze, J. Viljakka, M. Virkki, C.-Y. (D.) Huang, S. Hecht, A. Priimagi, *Chem. Sci.* **2023**, *14*, 2482.
[43] W. E. Benjamin, D. R. Veit, M. J. Perkins, E. Bain, K. Scharnhorst, S. Mcdowall, D. L. Patrick, J. D. Gilbertson, *Chem. Mater.* **2014**, *26*, 1291.
[44] H. Wang, K.-F. Xue, Y. Yang, H. Hu, J.-F. Xu, X. Zhang, *J. Am. Chem. Soc.* **2022**, *144*, 2360.
[45] V. Sharma, U. Puthumana, P. Karak, A. L. Koner, *J. Org. Chem.* **2018**, *83*, 11458.
[46] H. Liu, G. Yin, Q. Li, G. Liu, S. Pu, H. Zhang, *Dyes Pigments* **2019**, *165*, 319.
[47] L. Ceamanos, Z. Kahveci, M. López-Valdeolivas, D. Liu, D. J. Broer, C. Sánchez-Somolinos, *ACS Appl. Mater. Interfaces* **2020**, *12*, 44195.
[48] J. Cunha, T.-L. Guo, G. Della Valle, A. N. Koya, R. Proietti Zaccaria, A. Alabastri, *Adv. Opt. Mater.* **2020**, *8*, 2001225.
[49] A. Kotikian, C. Mcmahan, E. C. Davidson, J. M. Muhammad, R. D. Weeks, C. Daraio, J. A. Lewis, *Sci. Robot.* **2019**, *4*, eaax7044.
[50] Z. Deng, H. Zhang, A. Priimagi, H. Zeng, *Adv. Mater.* **2023**, https://doi.org/10.1002/adma.202209683.
[51] L. Ceamanos, D. J. Mulder, Z. Kahveci, M. López-Valdeolivas, A. P. H. J. Schenning, C. Sánchez-Somolinos, *J. Mater. Chem. B* **2023**, *11*, 4083.